Atlas-Based Segmentation of Pathological MR Brain Images Using a Model of Lesion Growth

Meritxell Bach Cuadra*, *Student Member, IEEE*, Claudio Pollo, Anton Bardera, Olivier Cuisenaire, *Member, IEEE*, Jean-Guy Villemure, and Jean-Philippe Thiran, *Senior Member, IEEE*

Abstract—We propose a method for brain atlas deformation in the presence of large space-occupying tumors, based on an *a priori* model of lesion growth that assumes radial expansion of the lesion from its starting point. Our approach involves three steps. First, an affine registration brings the atlas and the patient into global correspondence. Then, the seeding of a synthetic tumor into the brain atlas provides a template for the lesion. The last step is the deformation of the seeded atlas, combining a method derived from optical flow principles and a model of lesion growth. Results show that a good registration is performed and that the method can be applied to automatic segmentation of structures and substructures in brains with gross deformation, with important medical applications in neurosurgery, radiosurgery, and radiotherapy.

Index Terms—Atlases, magnetic resonance (MR) imaging, pathological brains, registration, segmentation.

I. INTRODUCTION

PRECISE segmentation of functionally important brain anatomical structures is of major interest in the minimally invasive approaches to brain space-occupying lesions treatment, including tumors and vascular malformations. It aims to reduce the morbidity or mortality and to improve the outcome of surgical, radiosurgical, or radiotherapeutic management of such lesions. Despite the spatial information and higher anatomical resolution provided by magnetic resonance (MR) imaging, precise visual segmentation may be a difficult task when anatomic structures are shifted and deformed. The use of deformable models to segment and project structures from a brain atlas onto a patient's MR image is a widely used technique. However, when large space-occupying tumors or lesions drastically alter shape and position of brain structures and substructures, these methods have been of limited use.

The purpose of this work is to deform a brain atlas onto a patient's MR image in the presence of large space-occupying meningiomas by explicitly modeling the tumor growth.

*M. Bach Cuadra is with the Signal Processing Institute (ITS), Swiss Federal Institute of Technology (EPFL), CH-1015 Lausanne, Switzerland (e-mail: Meritxell.Bach@epfl.ch).

A. Bardera, O. Cuisenaire, and J.-P. Thiran are with the Signal Processing Institute (ITS), Swiss Federal Institute of Technology (EPFL), CH-1015 Lausanne, Switzerland (e-mail: Olivier.Cuisenaire@epfl.ch; JP.Thiran@epfl.ch).

C. Pollo is with the Department of Neurosurgery, Lausanne University Hospital (CHUV), CH-1011 Lausanne, Switzerland, and also with the Signal Processing Institute (ITS), Swiss Federal Institute of Technology (EPFL), CH-1015 Lausanne, Switzerland (e-mail: Claudio.Pollo@chuv.hospvd.ch).

J.-G. Villemure is with the Department of Neurosurgery, Lausanne University Hospital (CHUV), CH-1011 Lausanne, Switzerland.

Digital Object Identifier 10.1109/TMI.2004.834618

To the best of our knowledge, only two approaches related to atlas-based segmentation on pathological brains have been published. Kyriacou *et al.* [1] propose to use a biomechanical model of the brain implemented using the finite-element method. The soft tissue deformations induced by the tumor growth are modeled first. Then, the nonrigid registration matches the anatomical atlas with a transformed patient image from which the tumor was removed. On the other hand, Dawant *et al.* [2] rely on a simpler approach based on optical-flows—Thirion's demons algorithm [3]—for both tumor growth modeling and atlas matching deformations. Their solution is called *seeded atlas deformation (SAD)*, as they put a *seed* with the same intensity properties as the lesion in the atlas image, then compute the nonrigid registration. Unfortunately, this requires to use a large seed that masks atlas structures, potentially leading to erroneous results. In [4], we presented preliminary results with an improved seeding procedure, i.e., using a smaller seed, but it still masks some atlas structures.

The approach presented in this paper is also inspired by the works of Dawant *et al.* [2], but introduces a number of important changes. Instead of applying the nonlinear registration algorithm to the whole image, we use a specific *a priori* model of tumor growth inside the tumor area, which assumes that the tumor has grown radially from a single voxel seed. Compared to previous approaches, this minimizes the amount of atlas information that is masked by the tumor seed. It also allows to use a single nonlinear registration step with adaptive regularization instead of the two steps approach advocated by Dawant. A further improvement comes from the automation of the segmentation of the patient's lesion. Finally, we propose a new validation method using a synthetic patient-specific atlas. This distinguishes between deformations due to interpatient anatomical variability and those induced by the tumor growth. Results obtained on real patient images and the assessment of these results by an expert show that atlas registration onto the MR image of a patient with large space-occupying lesions can be correctly performed.

This paper is organized as follows. In Section II, we detail the relevant state of the art, i.e., Thirion's demons algorithm, Kyriacou's biomedical deformation model, and Dawant's seeded atlas deformation. Section III describes our method in details. In Section IV, it is applied to patient data and results are discussed qualitatively. They are further validated in Section V. Finally, those results are extensively discussed in Section VI.

II. STATE OF THE ART

Atlas-based medical image segmentation techniques have been widely studied in the literature [5]. These techniques

convert the segmentation of a MR image into a nonrigid registration problem between the MR image of the patient and the MR image used to create the brain atlas. An exhaustive review of these techniques is beyond the scope of this paper. Instead, we present first a brief introduction to the demons algorithm [3], [6], the nonrigid registration technique for healthy brain images that serves as the basis for this paper as well as for [2], [4]. Then, we describe the approaches of Kyriacou [1] and Dawant [2], both dealing with the problem of atlas-based segmentation for pathological brains.

A. The Demons Algorithm

The *demons* algorithm [3], [6] approaches the problem of image matching as a diffusion process, in which object boundaries in the reference image F are viewed as semipermeable membranes. The other (so-called floating) image G is considered as a deformable grid, and diffuses through these interfaces driven by the action of effectors situated within the membranes. These effectors are also called *demons* by analogy with Maxwell's demons.

Various kinds of *demons* can be designed to apply this paradigm to specific applications. In the particular case of voxel-by-voxel intensity similarity, the *demons* paradigm is similar to optical flow methods. In this paper, the instantaneous force (velocity) for each demon point, $\vec{p}$ at the iteration $i + 1$ is

$$\vec{v}^{i+1} = \frac{\left(G\left(\vec{p} + \vec{D}^i(\vec{p}) \right) - F(\vec{p}) \right) \vec{\nabla} F(\vec{p})}{\left| \vec{\nabla} F(\vec{p}) \right|^2 + \left(G\left(\vec{p} + \vec{D}^i(\vec{p}) \right) - F(\vec{p}) \right)^2} \quad (1)$$

where $F(\cdot)$ and $G(\cdot)$ are the image intensities and $\vec{D}^i$ is the current displacement field. Thus, there is a displacement in the direction of the reference image gradient if there is both a difference in image intensities and a reference image gradient different from zero.

The deformation field is then computed from the instantaneous velocity by assuming that the two images to match are two frames separated by a unit of time

$$\vec{d}^{i+1} = \vec{D}^i + \Delta t \cdot \vec{v}^{i+1} \quad (2)$$

where $\Delta t = 1$.

Note that (1) is asymmetrical, that is, it gives different results depending on which image is chosen as the reference and which is chosen to be floating. In [3], Thirion presented a solution to provide *bijectivity* to the *demons* algorithm, and therefore, to provide a way of finding the *inverse* transformation. This is done by computing at each iteration both the *direct* deformation field [$\vec{d}_{\text{direct}}$, from (1) and (2)] and the *inverse* deformation field [$\vec{d}_{\text{inverse}}$, also from (1) and (2) but replacing F instead of G and vice versa]. Then, a residual vector field $\vec{R} = \vec{d}_{\text{direct}} + \vec{d}_{\text{inverse}}$ is equally distributed onto the two deformation fields

$$\vec{D}*^{i+1}_{\text{direct}} = \vec{d}^{i+1}_{\text{direct}} - \frac{\vec{R}}{2}$$

$$\vec{D}*^{i+1}_{\text{inverse}} = \vec{d}^{i+1}_{\text{inverse}} - \frac{\vec{R}}{2}. \quad (3)$$

In this approach, global smoothness of the total displacement field is not implicitly enforced. Locally similar displacements

for nearby voxels are imposed by smoothing both direct and inverse displacement fields with a Gaussian filter, i.e.,

$$\vec{D}_\alpha = \vec{D}*^{i+1}_\alpha \circ G(\sigma) \quad (4)$$

where $\vec{D}*$ is the deformation field at the current iteration, α refers to *direct* and *inverse*, $G(\sigma)$ is the Gaussian filter with standard deviation σ, and $\vec{D}$ is the regularized deformation field that will be used in (1) in the next iteration. It can be shown that if the instantaneous displacement field $(\vec{d})$ is filtered, a fluid deformation is obtained; while if the total field $(\vec{D}*)$ is filtered, it corresponds to an elastic deformation [7]. The choice of the smoothing parameter σ of the filter is a critical issue that has been studied in [8]. In the next section, we apply the nonrigid registration as an elastic process and, therefore, we also call σ the *elasticity parameter*.

Unfortunately, although it has been successfully applied to the registration of brain atlases with MR images of healthy volunteers or patients with nondeforming pathologies, this method cannot be applied as such in the presence of tumors. First, large morphological differences between image volumes render optical flow methods ineffective, although the algorithm can be made somewhat more robust if it is applied hierarchically. Second, the algorithm can only match objects that exist in both images, which is not the case for tumor brains, since there are no voxels with tumor-like intensities in the atlas image.

B. Nonlinear Elastic Registration

A first approach of registration with anatomical atlas for pathological brains was presented by Kyriacou *et al.* [1] in 1999. Their method is based on a biomechanical model of the brain using finite-element method. The soft tissue deformations induced by the growth of a tumor are modeled first. Then, they proceed to the registration with the anatomical atlas. The method can be summarized as follows.

1) An estimate of the anatomy prior to the tumor growth is obtained through a simulated contraction of the tumor region, using finite-elements and knowing the position of the skull, ventricles and the falx and tentorium. It results in an estimation of the patient anatomy before the lesion growth.

2) This estimated tumor-less patient is treated like a healthy brain. A *normal* to *normal* atlas registration is performed using an elastic deformable model.

3) The estimation of the tumor growing process is applied to the registered atlas. That is not performed using the inverse transformation found in the first step but applying a nonlinear regression method driven by distinct anatomical features that are used to estimate the origin of the tumor and the level of strain.

This method presents good results, but has some important drawbacks. The model for tumor growth has a tendency on uniform growth. Also, it requires the previous accurate segmentation of many structures in order to perform the nonlinear regression estimation. Finally, due to some implementation difficulties such as computational requirements, mesh generation and visualization, the method has only been implemented in two dimensions while the problem is by nature three-dimensional.

C. Seeded Atlas Deformation Method (SAD)

The other attempt at atlas registration for pathological brains was introduced by Dawant *et al.* [2]. It is a simpler approach where both the tumor deformation and the inter-patient variability are handled by a modified *demons* algorithm. The presence of the tumor is modeled by introducing synthetic lesion voxels—the seed—in the atlas MRI. Indeed, there needs to be at least some voxels with tumor-like intensities in the atlas MRI in order to trigger the demons movements. Besides, the seed cannot be too small compared to the tumor as this would violate excessively the assumption of small displacements. Practically, the algorithm works as follows.

1) Apply bijective *demons* algorithm in a very rigid way ($\sigma = 2.0$ mm) to warp the brain atlas onto the patient's image.
2) Insert the lesion template into the warped brain atlas in order to get a *seeded* atlas MRI.
3) Apply bijective *demons* algorithm in a very elastic way ($\sigma = 0.5$ mm), to warp the *seeded* atlas MRI onto the patient's image.

This method succeeds reasonably well at forcing the demons to move similarly to the lesion growth. Unfortunately, it presents an important drawback because the seed needs to have a considerable size to obtain a reasonable modeling of the tumor growth. Thus, the anatomical information masked by the seed cannot be recovered and produces errors in the segmentation. Also, it turns out that the seed deformation is strongly dependent on both the number of iterations of the algorithm and the choice of the elasticity parameter.

III. METHOD

Our approach to brain atlas deformation in the presence of space occupying tumors is based on Dawant's SAD algorithm [2] but differs from it on three major points. First, segmentation of the patient's lesion is performed automatically, instead of manually. Second, an *a priori* model of radial tumor growth is applied inside the lesion area. Third, the algorithm is implemented in a single step thanks to the introduction of an adaptive Gaussian filtering. Our method, which we call *model of lesion growth (MLG)*, works in four steps.

1) An affine transformation is applied to the atlas image in order to globally match the patient.
2) The lesion is segmented using the adaptive template moderated spatially varying statistical classification (ATM SVC) algorithm.
3) The atlas is manually seeded by an expert with a single voxel placed on the estimated origin of the patient's lesion.
4) The nonlinear demons registration algorithm with MLG is performed in order to deform the seeded atlas to match the patient.

After applying these steps, we have a deformed brain atlas image in which the tumor has grown from its seed, causing displacement and deformation to the surrounding tissues. Structures and substructures from the brain atlas may then be
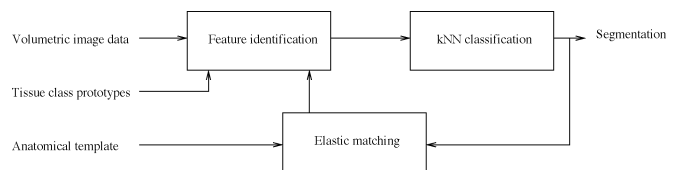

Fig. 1. Scheme for the ATM SVC algorithm.

projected to the patient's image using the same displacement field. We now detail these four steps.

A. Affine Transformation

Before performing the nonrigid deformation, it is necessary to bring the atlas and patient volumes into global correspondence. Indeed, the demons algorithm requires having at least a partial overlap of the corresponding patient and atlas structures in order to match them.

As proposed by Cuisenaire *et al.* [9], the global transformation $y = T(x)$ from the patient cortical surface to the atlas cortical surface is modeled by a linear combination of N elementary scalar functions $f_j(x)$ for each coordinate $y_i (i = 0, 1, 2)$ of y. These functions are decorrelated, then the coefficients of the linear combination are optimized in order to minimize the Euclidean distance between the atlas cortical surface and the correspondent cortical surface in the target image. These surfaces are previously segmented using simple morphological operations [10]. Here, we restrict ourselves to an affine transform, i.e., to $N = 4$ and $f_j(x) = 1, x_0, x_1, x_2$.

B. Lesion Segmentation

The patient's lesion needs to be segmented in order to specify the volume in which the model of tumor growth will be applied. To this purpose, we use a variant of the ATM SVC algorithm proposed by Warfield *et al.* [11], [12]. This algorithm uses both image and anatomical information embedding them in a high dimensionality space in which a k-nearest neighbors (k-NN) classification is performed. One dimension of this feature space is the image intensity. The other dimensions are the distances to the structures from a brain atlas warped onto the corresponding structures classified from the patient image. The algorithm is implemented in a hierarchical way, so that the dimensionality of the feature space and the number of classified structures increase progressively at each level.

- Level 1: The intensity feature is used for the classification into the *brain* and the *background* classes.
- Level 2: The intensity and distance to the brain surface are used to classify the *ventricles*, *brain*, and *background*.
- Level 3: Intensity, distance to the brain and distance to the ventricles are used for the classification into *lesion*, *ventricles*, *brain*, and *background*.
- Level 4: Intensity, distance to the brain, distance to the ventricles, and distance to the lesion contour are used for the final classification into *lesion*, *ventricles*, *brain*, and *background*.

In the first level, the classification is done by simply binarization of the image. In the levels 2, 3, and 4, the process represented in Fig. 1 is applied. We use the demons algorithm as elastic matching instead of the one used in [11] and [12]. Note that the
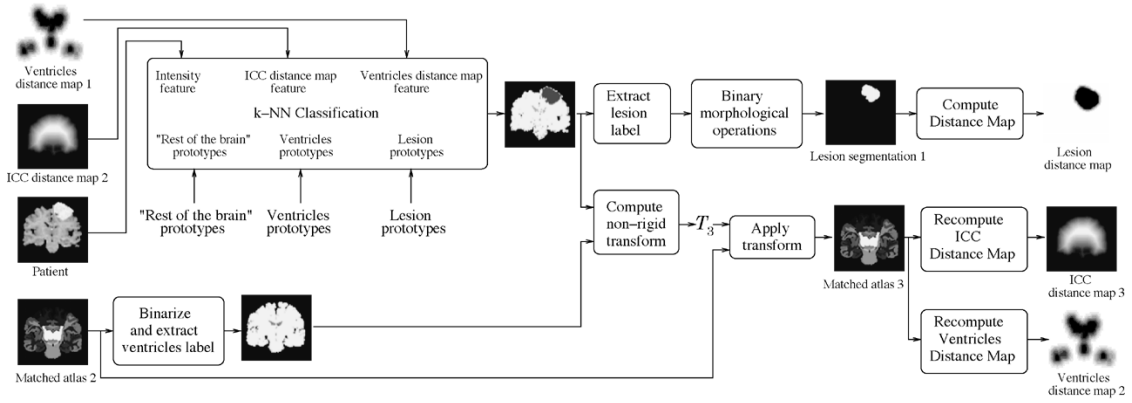
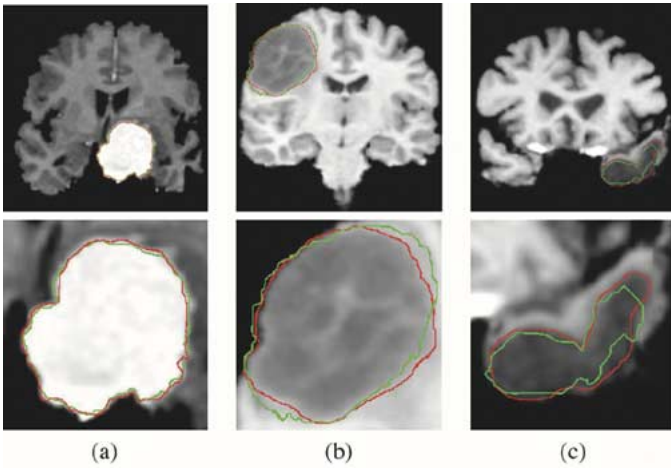Fig. 2.   Third level of the ATM SVC classification algorithm.

Fig. 3.   Segmentation results obtained with the ATM SVC algorithm on various lesion and tumor types. Red: manual segmentation. Green: ATM SVC segmentation. (a) Meningioma with left parasellar location. (b) Low-grade glioma with right frontal location. (c) Cardiovascular accident (CVA), also called stroke.

distance to the brain surface and to the ventricles is computed from the registered atlas while the distance to the lesion is computed from the classified patient (see Level 3 in Fig. 2).

In Fig. 3, we compare the results for various lesion types of the ATM SVC segmentation with those of a manual segmentation performed by experts (green and red contour, respectively). These results were obtained with $k = 7$ for the k-NN classification, and using 100 prototypes (manually chosen) for each one of the classes. A detailed description of our ATM SVC implementation can be found in [13].

C. Atlas Seeding

After the affine transformation, the atlas and patient volumes are globally in correspondence except in regions that have been drastically deformed by the tumor. We proceed to the atlas seeding by manually selecting the point of origin of the tumor growth in the affine-registered brain atlas.

Both our previous work [4] and Dawant's [2] use an extended seed in order to drive the tumor deformation. It makes the positioning of the seed a relatively easy task but unfortunately masks atlas structures under the seed. In this paper, the single-

voxel seed induces no masking but—as will be discussed in Section V—the selection of the correct seed location requires anatomical and biological knowledge of tumor growth.

D. Nonrigid Deformation Using a Model of Tumor Growth

At this point, the affine registration ensures that the small displacement assumption is respected in the region of the brain that is far from the tumor. Meanwhile, the segmentation of the tumor volume and the manual selection of the tumor seed provide an adequate model for the tumor and its influence on immediately surrounding tissues.

The nonrigid deformation method we propose distinguishes between those two areas fixed from the lesion segmentation. Outside the lesion, the *demons* force as defined in (1) is applied. Inside the lesion, the tumor growth model assumes a *radial* growth of the tumor from the tumor seed, i.e.,

$$\overrightarrow{v}_{\text{lesion}}^{i+1}(\vec{p}) = \frac{\overrightarrow{DM}_{\text{seed}}}{N_{it}} \tag{5}$$

where $\overrightarrow{v}_{\text{lesion}}$ is the instantaneous velocity inside the lesion area, $\overrightarrow{DM}_{\text{seed}}$ is the distance from the corresponding point $\vec{p}$ to the seed, and N_{it} is the number of iterations of the deformation algorithm that have to be performed. Then, the deformation field $\overrightarrow{d}_{\text{lesion}}^{i+1}$ is computed similarly as in (2). The bijectivety inside the lesion area is ensured by forcing $\vec{d}_{\text{direct}} = -\vec{d}_{\text{inverse}}$. This model allows the points inside the tumor to converge toward the seed voxel,[1] while remaining simple and allowing any number of iterations to take place outside the tumor volume.

The displacement vector computed at every voxel using either the demons force (1) or the tumor growth model (5) is regularized by an adaptive Gaussian filter to avoid possible discontinuities. Three areas are considered: inside the lesion area, close to the lesion (within 10 mm of the tumor) where large deformations occur, and the rest of the brain. Smoothing is not necessary inside the lesion because the vector field induced by (5) is highly regular and the continuity is ensured. So, $\sigma = 0$ inside the lesion area. In the region close to the tumor (including the tumor contour), there are large deformations due to the tumor growth. Then, it is necessary to allow large elasticity, i.e., σ should have

---

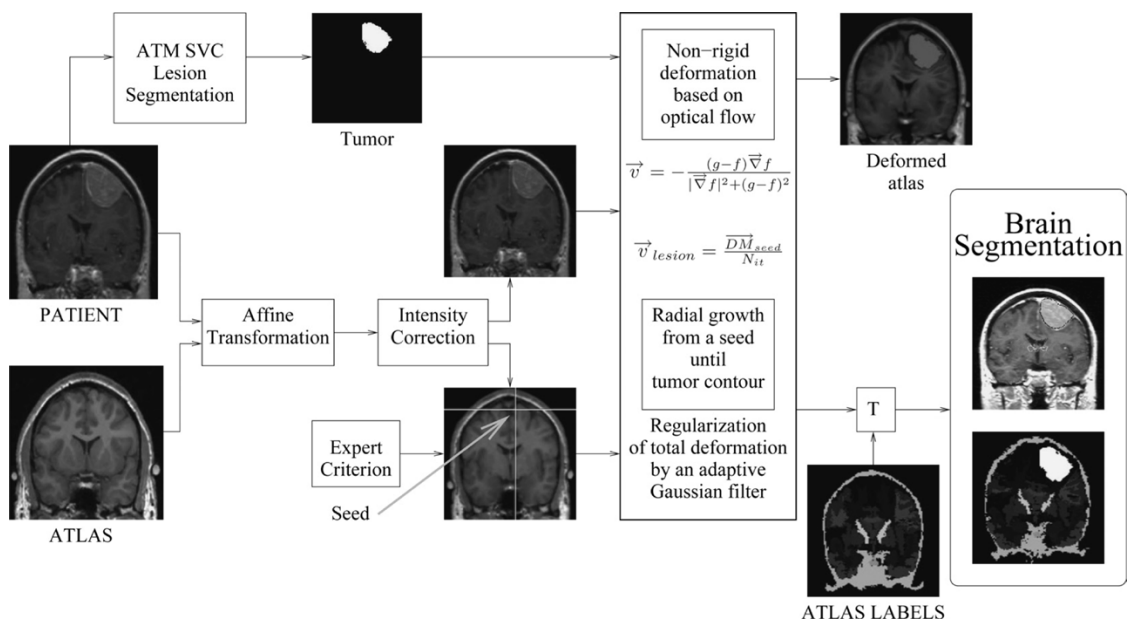[1]Notice that the vector field points the origin, and not the destiny, of a voxel.

Fig. 4. Block diagram of the atlas-based segmentation method using a model of lesion growth (MLG algorithm). Note that, because of limited space, $F(\vec{p})$ and $G(\vec{p} + \vec{D}^i(\vec{p}))$ [see (1)] are denoted here by f and g, respectively.
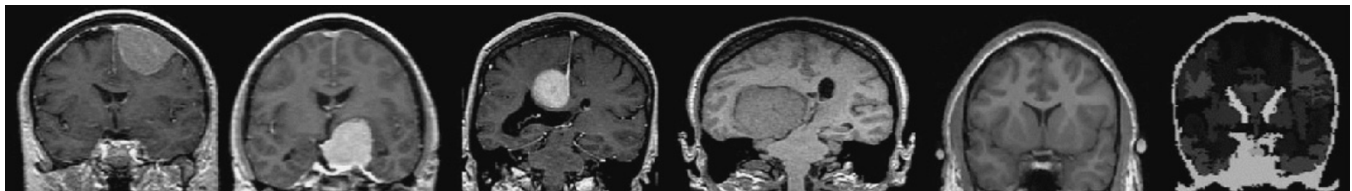

Fig. 5. Coronal slices of the data set. From left to right: patients from 1 to 4, atlas MRI and atlas labels.

a small value, typically 0.5 mm. In the rest of the brain, deformations are smaller, due primarily to interpatient anatomical variability. So, a larger σ proves to be better, as it simulates a more rigid transformation. Previous studies [8] suggest that a typical σ to match two healthy brains is about 0.5 and 1 mm. In what follows, $\sigma = 0.8$ mm is used. The number of iterations is arbitrarily fixed to $256 + 128 + 32 + 16$ from low to high resolution scale.[2] The algorithm stops at the end of the iterations.

IV. RESULTS

A. Data Sets

The patient images used in this study have been retrieved from the Surgical Planning Laboratory (SPL) of the Harvard Medical School and NSG Brain Tumor Database [14] and also from the Department of Radiology of the Lausanne University Hospital. They consist of 4 volumes of 128 coronal slices of 256×256 pixels and $0.9375 \times 0.9375 \times 1.5$ mm^3 of voxel size. All of them present a meningioma. This kind of tumor is usually benign and its extracerebral growth usually induce a pure shift and deformation of the underlying brain structures (see patient MR images on Fig. 5). Meningiomas are lesions of interest because they are typically suitable for radiosurgery

[2]The algorithm is implemented in a multiscale way: a first match is made with downsampled images and the resulting transformation is upsampled to initialize the next match with finer image resolution.

or stereotactic radiotherapy. No brain edema was observed on the data set. Notice that most of the patient images have been acquired using a contrast agent.

The digital atlas used in this work comes from the SPL [15]. It is composed of two images: an MRI and a *label* image. The MRI has been made of MR data from a single normal subject scanned with high resolution $256 \times 256 \times 160$ volume data set in coronal orientation with $0.9375 \times 0.9375 \times 1.5$ mm^3 voxel size. The label atlas image contains anatomical and functional structures that have been manually segmented (see Fig. 5).

B. Deformed Atlas Images and Deformation Field

The MLG deformation is analyzed by comparing it to Dawant's SAD [2]. Because of limited space, only the study for one patient (Patient 2, Fig. 5) is presented. Similar results have been obtained for the other patients of the data set. Patient 2 has a left parasellar meningioma of approximately dimensions $41 \times 42 \times 52$ mm^3. We have applied the SAD method for two different seed sizes [resulting from the tumor mask erosion of 8 and 12 mm, respectively, see Fig. 6(a) and (b)]. The MLG has been run as presented in Fig. 4 and using the parameters defined in Sections III-B and III-D. In Fig. 6(c) the one-voxel seeded atlas is shown.

Fig. 6(g), (h), and (i) represents the vector field of the SAD and the MLG respectively, and Fig. 6(j), (k), and (l) represents
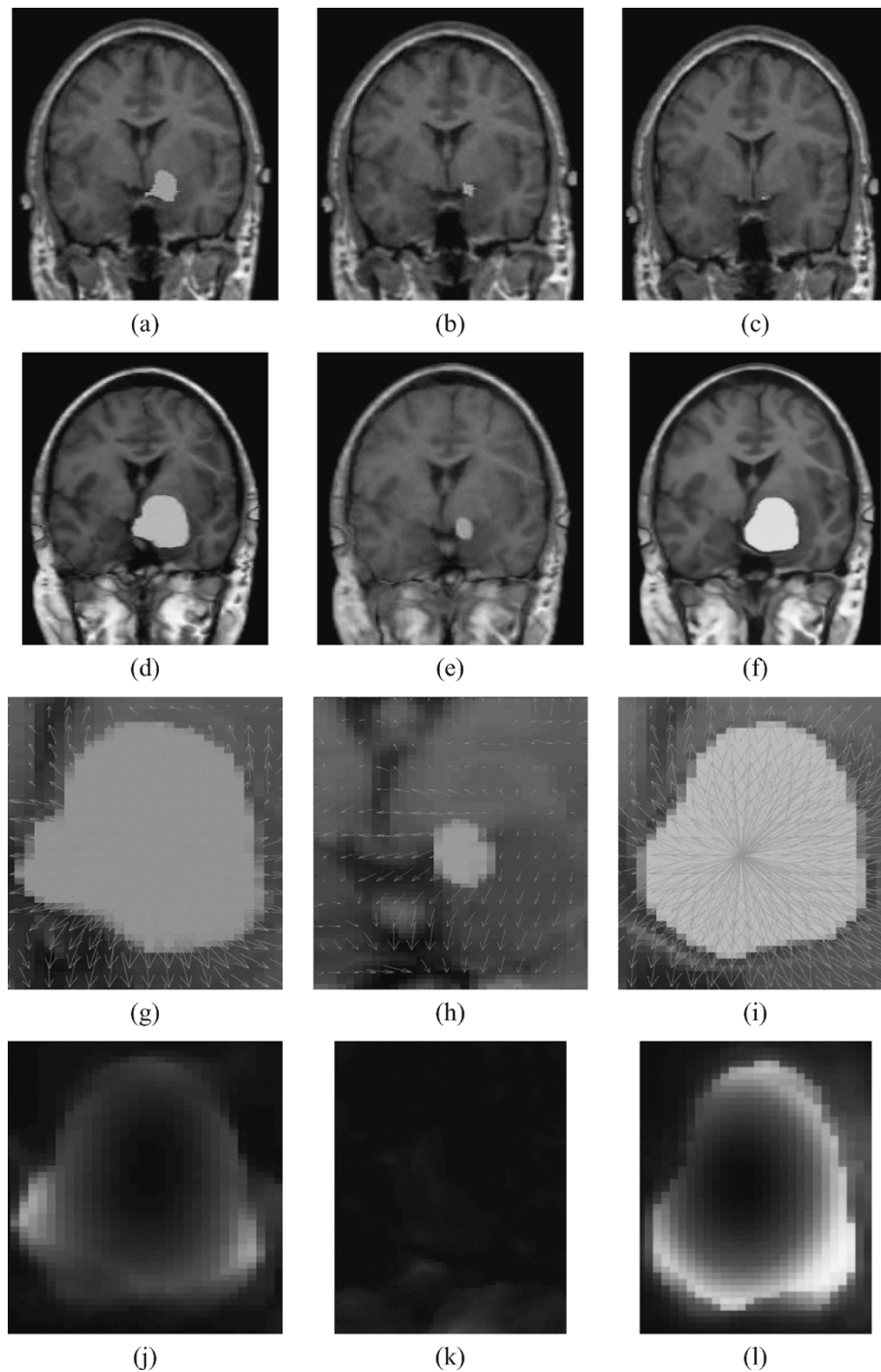
Fig. 6.   Atlas seeding, lesion growth and deformation field analysis. (a) Seeded atlas, large seed. (b) Seeded atlas, small seed. (c) Seeded atlas, one voxel seed (in green). (d) Deformation of seeded atlas with the large seed using SAD. (e) Deformation of seeded atlas with the small seed using SAD. (f) Deformation of seeded atlas with one voxel seed using MLG. (g) SAD: deformation field using a large seed. (h) SAD: deformation field using a small seed. (i) MLG: deformation field. (j) SAD: norm of deformation field using a large seed. (k) SAD: norm of deformation field using a small seed. (l) MLG: norm of deformation field. Note: Deformation field corresponds to a zoom of the lesion. Brightest areas correspond to largest deformation.

the norm of the deformation of the SAD and the MLG respectively. We can see that the performance of SAD when using the largest seed is, in terms of deformed atlas and deformation field, comparable to the performance of the MLG. Note that the deformation field is almost the same for both methods [cf. Fig. 6(d) and (f)]. However, when using the small seed, the deformation obtained by the SAD method inside the tumor area does not reach the tumor border [Fig. 6(e)]. The force inside the lesion area is actually misguided as we can see in Fig. 6(h) and (k).

The different behavior between the two approaches can be explained as follows. The SAD highlights the tumor and seed masks to obtain a strong gradient on the tumor and seed contours. But between them, only the intensity gradient of the atlas MRI is used since intensity gradient within the highlighted tumor area is zero. Having only gradient information on the contours is not strong enough when using a small seed since a large deformation is needed to make the seed grow toward the tumor. Furthermore, that explains the dependency of the SAD
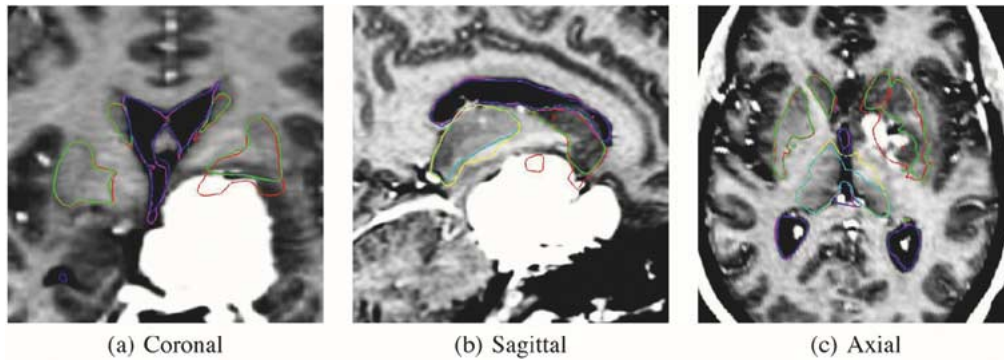
Fig. 7. Patient 2: ventricles (MLG in blue, SAD in magenta), thalamus (MLG in cyan, SAD in yellow), and central nuclei (MLG in green, SAD in red). (a) Coronal. (b) Sagittal. (c) Axial.

method on the seed size and iteration number. On the contrary, the MLG can compensate the large anatomical differences between the one-voxel seed and the tumor thanks to *a priori* information from the growth model.

C. Segmentation Results Study

1) Importance of the Tumor Growth Model: The above section may be too critical of SAD. Indeed, it would not really matter that SAD fails to grow the tumor to its full size if this did not affect the deformation of the structures of interest around it. Hence, in this section we compare MLG and SAD with a small seed according their ability to segment such structures, i.e., the ventricles, the thalamus, and the central nuclei.

The coronal, sagittal, and axial view of these segmentations are shown in Fig. 7. The ventricles are almost exactly segmented by both approaches. The thalamus segmentation is performed slightly better by MLG than by SAD. Their differences can be appreciated in Fig. 7(b) and (c). The most critical structure is the central nuclei for which the atlas structure after affine registration overlaps with the tumor. In this case, SAD fails and the central nuclei segmentation remains inside the tumor volume. On the contrary, MLG correctly pushes the central nuclei out of the tumor region which improves the segmentation. This shows the need of a correct estimation of the tumor growth in order to obtain a good final segmentation of the structures directly displaced and deformed by the lesion.

2) MLG Segmentation Results: Let us now consider the segmentation results for all the patients of the data set with the MLG algorithm. For this purpose, structures of interest from the deformed brain atlas have been projected to the patient images: the tumor (in red), the ventricles (in green), the thalamus (in yellow), and the central nuclei (in dark blue) (see Fig. 8).

Segmentations of both patient 1 and patient 2 are satisfactory [see Fig. 8(a) and (b)]. The structures have been correctly pushed outside the tumor area and the final deformation converges accurately to the target image. For these patients, all large anatomical differences between the patient images and the atlas can be attributed to the lesion and the influence of its growth on neighboring tissues.

The segmentation results for both patient 3 and 4 are less satisfactory [see red arrows in Fig. 8(c) and (d)]. These two cases are significantly more complex since large morphological differences exist between the atlas and the patients' brains in addition to the lesion. For instance, patient 3 also suffers from ventricular entrapment. For this patient, the structures of interest have been correctly pushed outside the lesion area, but some structures, particularly the ventricles, have not been correctly deformed. Our method considers a *normal* elasticity, and consequently *normal* deformation, in the regions far from the tumor while ventricular entrapment represent an abnormal dilatation of a portion of a ventricle that is progressively excluded from the ventricular system. In patient 4, the assumption of overlapping between same anatomical structures required by the demons algorithm has been largely violated. For example, the left ventricle of the atlas is actually placed over the right ventricle of the patient (see Fig. 9). This makes the nonrigid registration fail outside the lesion area even if the seed has correctly grown until the tumor edges.

D. Variation of the MLG Method

As we have seen in the previous section, in some cases, MLG fails when there are large morphological differences between the patient and the atlas in addition to the lesion itself. In these cases, the method can be improved as follows.

First, we apply the MLG algorithm as explained in Section III-D but in a very rigid way: $\sigma = 2$ mm far away from the lesion, $\sigma = 0.5$ mm near the lesion, and no filtering is applied inside. Moreover, the MLG uses a tumor mask that has been eroded (typically 3 mm) in order not to impose so much deformation next to the lesion area at a first time. So, a *rigid* matching between the main structures is done and a new *atlas* with a lesion template is obtained. Now, a nonrigid registration between two brains with an overlap between the corresponding structures (including the tumor) can be applied. Therefore the *demons* algorithm is valid for this objective. The algorithm is used in a elastic way ($\sigma = 0.7$ mm) because these brains have larger deformability than in the case of normal anatomy. Fig. 10 summarizes the performance of the new proposed algorithm. The *modified* MLG algorithm has been applied for patient 3 and patient 4. Segmentation results are shown in Fig. 11. Much better result is obtained for patient 3 [compare the arrows in Fig. 8(c) and Fig. 11(a)] where the ventricles displacement have been correctly match. However, no improvement has been obtained for patient 4. Neither the ventricles nor the central nuclei of the atlas overlap the patient structures. Notice that patient 4 is a very complex case since even the MSP, that is usually much more rigid than the brain tissues, has been largely deformed.

(a) Patient 1

(b) Patient 2
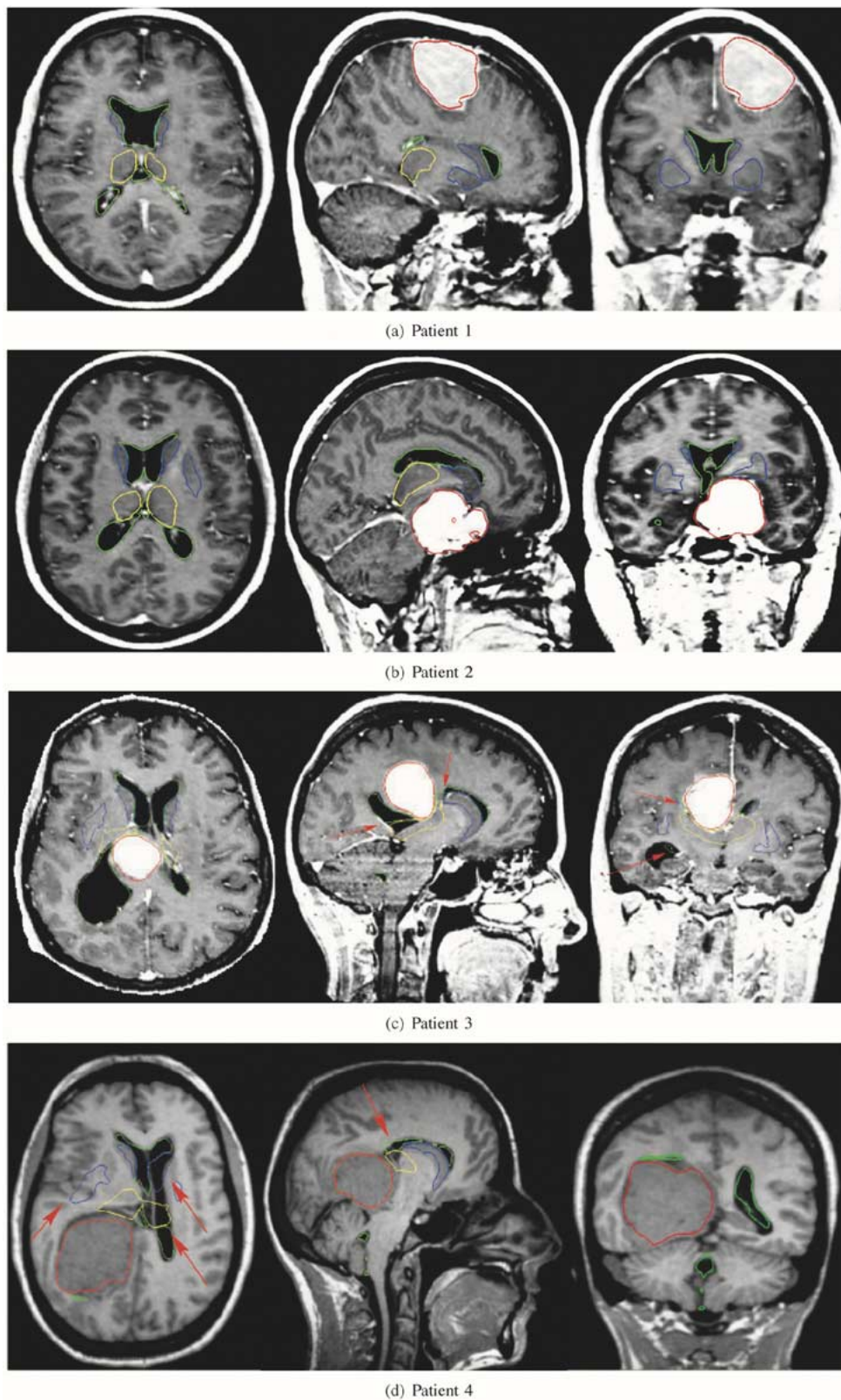
(c) Patient 3

(d) Patient 4

Fig. 8.   Segmentation results after applying the MLG algorithm. Displayed structures are: tumor (red), ventricles (green), thalamus (yellow), and central nuclei (blue). (a) Patient 1. (b) Patient 2. (c) Patient 3. (d) Patient 4.

In summary, we propose to apply the MLG *two steps* algorithm when large deformations exist in the patient brain moreover the lesion, and, the MLG *one-step* when the lesion is the main anatomical difference between the patient and the atlas.

V. VALIDATION

The lack of a gold standard for validation is one of the key problems of the nonrigid registration techniques in medical images. This problem is even more difficult in this case since two
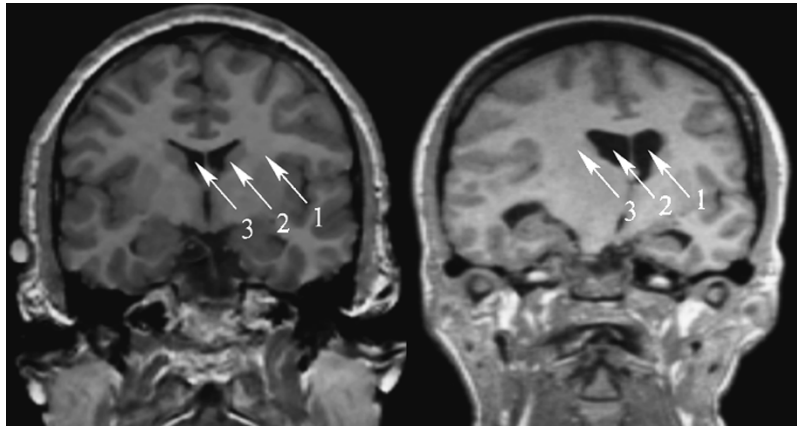
Fig. 9. Wrong initialization of MLG method for patient 4: the enumerated arrows represent the same spatial position. Note that anatomical structures do not correctly overlap.
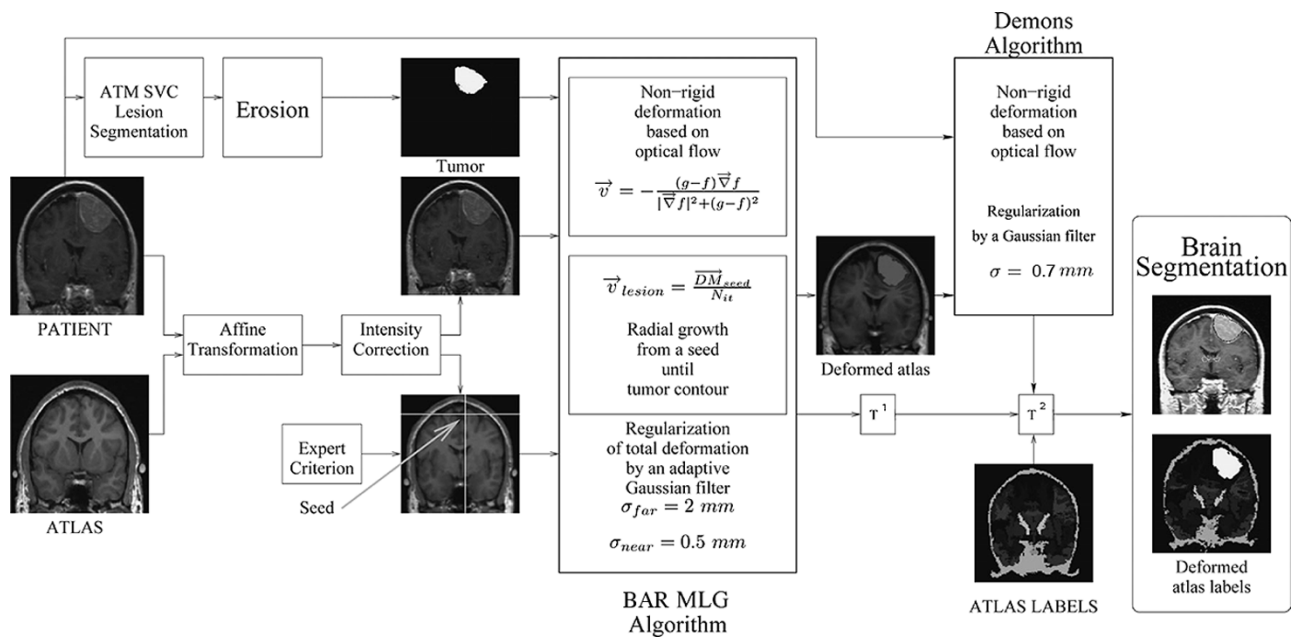

Fig. 10. Block diagram of the MLG *modified* algorithm.

different deformations occur: intersubject (or atlas-patient) variability and healthy to pathological warping. The validation of registration between healthy subjects is a very active research area [16]–[18]. However, the *demons* algorithm validation will not be treated in this paper.

In this section, we focus on how accurately the MLG can model the healthy to pathological warping. More precisely, our aim is twofold: validate not only the lesion growth but also the seed position.

A. Validation of the Lesion Growth

The validation method should demonstrate that our algorithm warps the brain in the same way as the growth of the lesion. To show it, our algorithm should be applied to the patient before the growth of the lesion but of course this information is not available. Thus, another question arises: how to have a good estimation of how the patient brain was before the appearance of the tumor. We know that the brain has approximately symmetrical structures. Therefore, the *damaged* hemisphere was almost

like the *healthy* one before the tumor grew. This idea is the basis of the validation, which goes as follows.

1) The brain *symmetry plane* that separates the right and the left hemispheres, called midsagittal plane (MSP), is found.
2) A *synthetic healthy* patient is created by mirroring the *healthy* hemisphere of the brain.
3) The MLG algorithm is applied between the patient and the synthetic healthy patient as explained in Section III-D.
4) The differences between the deformed synthetic healthy patient and the patient are evaluated.

To find the MSP, the mean square error (MSE) between both sides of the coronal plane is minimized. The tumor and its mirror are not taken into account because they do not have a symmetrical structure. The minimization algorithm used is the Powell algorithm as described in [19]. In Fig. 12, the MSP found for the Patient 2 is shown.

Once the symmetry plane is found, the *healthy* and the *damaged* hemispheres have been determined. To generate a new
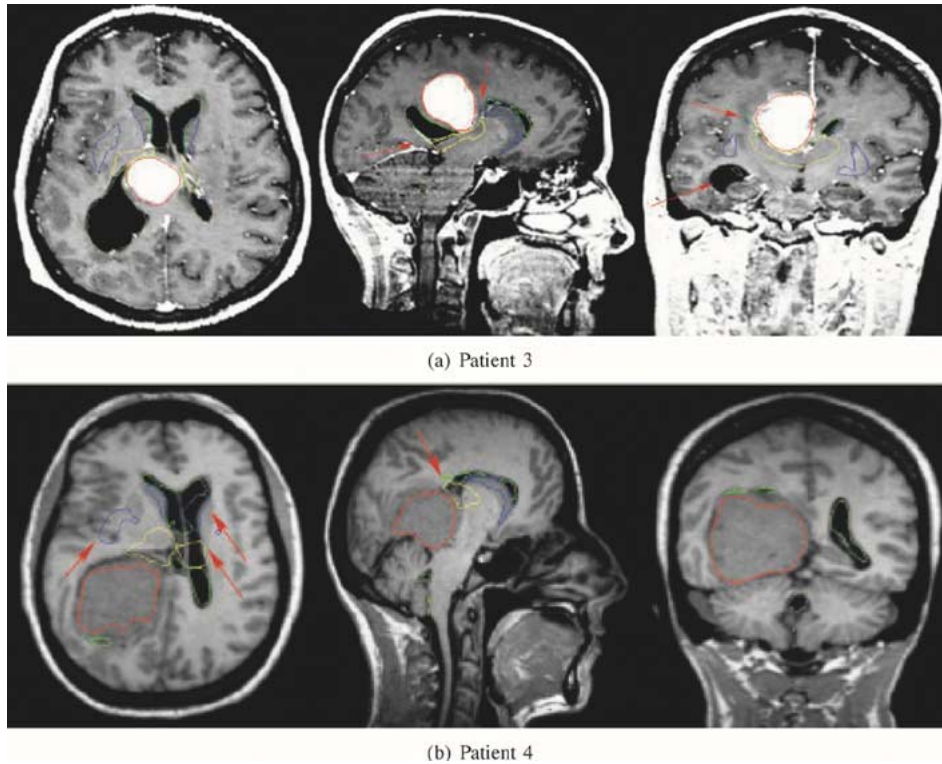
Fig. 11. Segmentation results after applying the MLG *modified* algorithm. Displayed structures are: tumor (red), ventricles (green), thalamus (yellow), and central nuclei (blue). (a) Patient 3; (b) patient 4.

synthetic patient-atlas, a simple mirroring of the *healthy* side is done. Note that, with this new atlas, the most similar brain a posteriori to the *healthy* brain of the patient is obtained. Only patients who do not present large deformations on the MSP and those who have a tumor only in one hemisphere of the brain can be used in this validation approach because of the mirroring step. Unfortunately, there is only one patient in our database fulfilling these conditions: patient 2 (Fig. 5). The result of the validation for this patient is presented in Fig. 12. It shows the warped synthetic atlas and the resulting segmentation of patient respectively. To obtain this final segmentation, a nonrigid matching between the digitized atlas and the *synthetic atlas* has been previously done in order to obtain a first segmentation of the *synthetic atlas*. Then, the transformation found by the MLG algorithm can be applied to the *synthetic atlas* image and a final segmentation of the patient is obtained. So, two transformations have been applied to the original atlas image. That means that, if there was some imprecision on the first nonrigid registration algorithm, the MLG method will propagate a wrong initial segmentation. But, according to the expert criteria, the final segmentation obtained for this case is correct. Of course, to obtain a more accurate assessment, the validation method we have proposed should be applied to many more cases.

B. Validation of the Seed Position

Seed position is a critical point of the MLG since it simulates where the tumor has begun to grow, and different choices of position may lead to very different results. To evaluate the influence of this parameter, MLG registration between *synthetic patient-atlas* and the patient was applied for six different initial

positions of the seed voxel chosen by the expert as possible origins of the tumor (see Fig. 13). The resulting deformation for each seed is shown in Fig. 14. The original patient and the resulting deformed *synthetic atlas-patient* are displayed. The seed position is represented by a little sphere. For this patient, the most *logical* position, under expert criteria, is the one placed at coordinates (205, 136, 47) [colored in magenta in Fig. 13 and Fig. 14(a)]. It is actually placed in the *middle* of the cerebral convexity since, in principle, no growing direction is more probable than others inside the brain.

First, we have visually validated the deformation by the assessment of an expert. The areas where the MLG method has performed correctly are marked using green arrows and the areas where MLG has not performed correctly using red arrows. The most *logical* seed position has correctly displaced gyri but it has also performed too much deformation at the MSG. That is because large elasticity near the lesion has been supposed while, in fact, in this case, the mid sagittal plane is near the lesion and it is a structure largely rigid. The rest of the seed positions, as desired, have not deformed too much the MSP [see Fig. 14(d) and (c)] but they have not correctly displaced the gyrus.

Second, the deformation error has been quantified calculating the MSE per voxel between the original patient and the deformed *synthetic* atlas-patient (see Fig. 14). A small MSE represents, for this particular case, a good deformation since the two images are supposed to be the same patient before and after the lesion growth and both images have the same intensity distribution. The lowest error is 34.08 for (205, 136, 47), the most *logical* initial seed position, and the largest error corresponds to (206, 139, 53). However, these values are not significantly
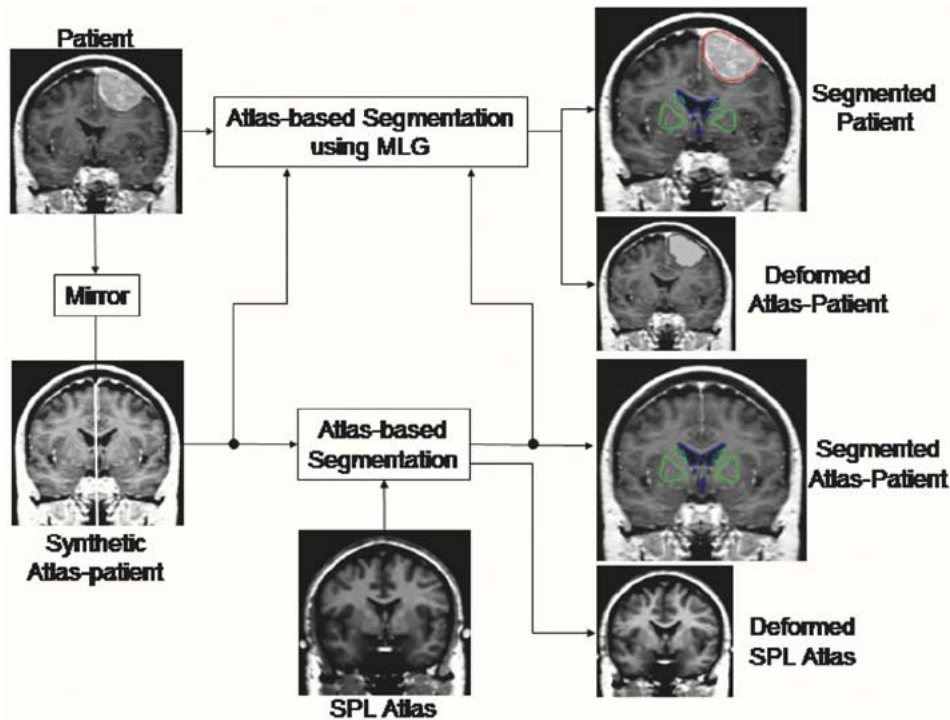
Fig. 12. Validation method results. Coronal view. Displayed structures: central nuclei (green), ventricles (blue) and tumor (red).
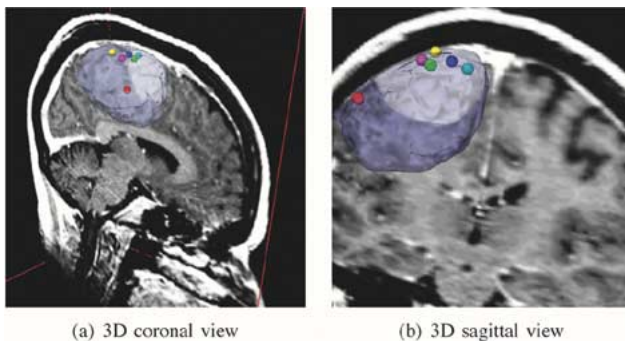

Fig. 13. Different locations of the initial seed. Magenta (205,136,47), red (192,119,38), green (205,131,50), cyan (205,137,57), yellow (207,145,48) and blue (206,139,53). (a) 3-D coronal view. (b) 3-D sagittal view.

different to conclude if one position performs much better deformation than another. In our opinion, MSE measure could be hardly used to validate the deformation in the case of interpatient matching because the images do not have a perfect intensity correspondence. Furthermore, even if we know the most probable initial position of the tumor in the *synthetic atlas-patient*, we cannot be sure that it will be exactly in the same position for the atlas since both, *synthetic atlas-patient* and atlas, are morphological and morphometrically different. Third, validation of segmentation for some interesting structures such as the ventricles, the thalamus, the central nuclei, and the tumor is performed. In Fig. 15 a global view of all the segmented structures superposed can be seen. Each color corresponds to the result of each seed position. Actually, not too much variability has been detected neither in the position nor in the morphology of the studied structures as expected [see the segmented thalamus in Fig. 16(b)]. However, there are some morphological differences when looking at the ventricles region [see Fig. 16(a)]. In

this case, almost all structures under study are quite far from the tumor, so they are not really influenced by the initial seed position. Only the ventricles seem to be more influenced by the seed since they are the most deformed structure due to the lesion growth.

Finally, statistics on volume (in mm^3) of the segmented structures have been calculated (see Table I). The structures that have the largest volume standard deviation due to different seed positions are the ventricles with a 0.35% and, the tumor with 0.18%. These measures confirm the visual validation on segmentation.

VI. DISCUSSION

The introduction of an explicit model of tumor growth (MLG) into the seeded atlas deformation (SAD) algorithm positively affects both the robustness of the method and its precision. The robustness is improved by removing parameters from the algorithm. While SAD requires a choice of seed shape and size, MLG does not as its seed is a single voxel. Also, the extent of the tumor growth with SAD is highly dependent on the number of iterations performed, while the explicit MLG grows to the whole tumor volume independently from this number.

Another important aspect of using the MLG is its effect on the regularization parameter σ used by the demons algorithm. SAD requires that only a mild regularization is applied in order to let enough flexibility for the demons algorithm to compensate the large shifts introduced by the tumor growth. This is a potential source of imprecision as optical flow algorithms can easily converge to a perfect match of image intensities that is not at all anatomically relevant. Anatomical relevance in such methods comes directly from a strong regularization step, with the assumption that a regular deformation field is very likely an anatomically relevant one. On the other hand, the MLG allows
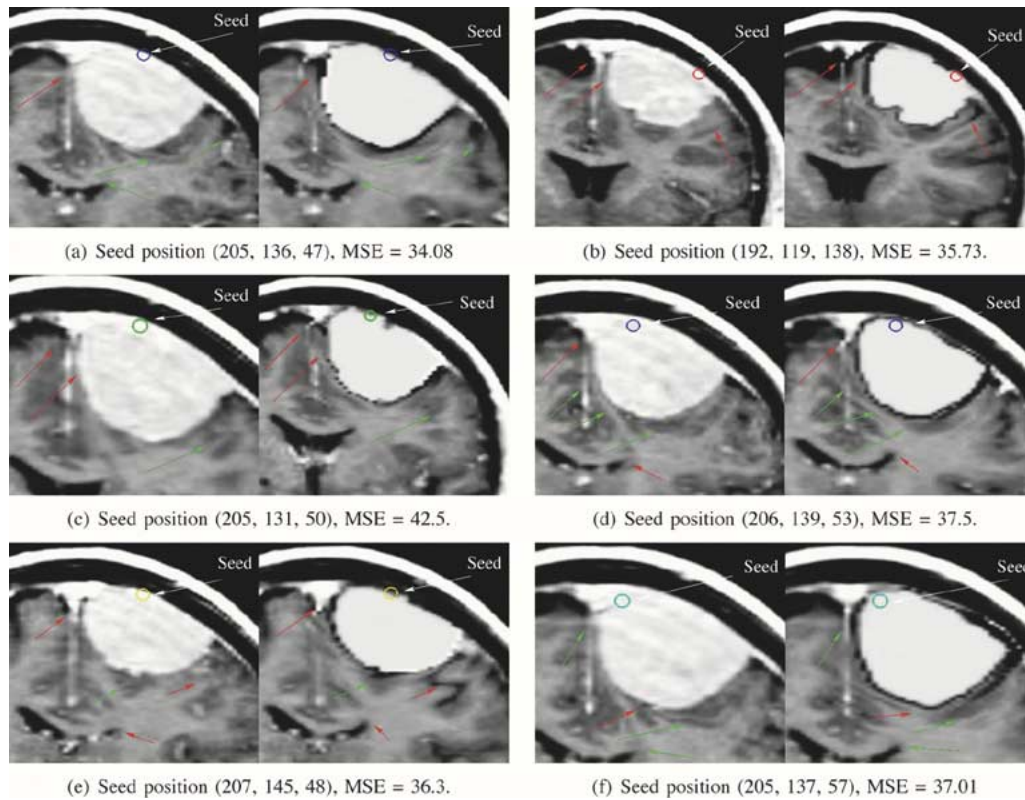
Fig. 14.   Preliminary study of the deformation variability depending on the seed position. MSE is the sum of squared differences per voxel between the original patient and the deformed synthetic patient-atlas. Green arrows denote the regions where MLG has deformed correctly. Red arrows denote the errors. (a) Seed position (205, 136, 47), MSE $= 34.08$. (b) Seed position (192, 119, 138), MSE $= 35.73$. (c) Seed position (205, 131, 50), MSE $= 42.5$. (d) Seed position (206, 139, 53), MSE $= 37.5$. (e) Seed position (207, 145, 48), MSE $= 36.3$. (f) Seed position (205, 137, 57), MSE $= 37.01$.
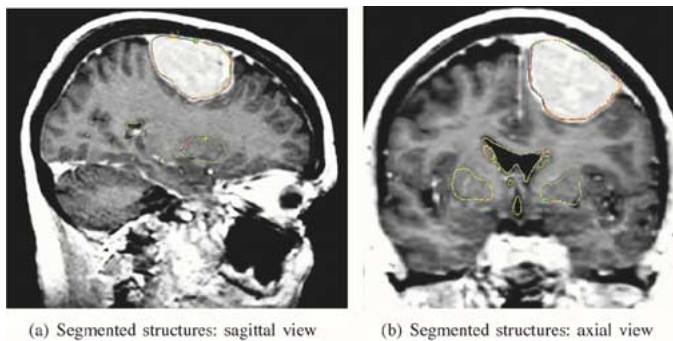

Fig. 15.   Segmentation results for each seed position. (a) Segmented structures: sagittal view. (b) Segmented structures: axial view.

us to keep regularization at a reasonable level. Furthermore, the introduction of adaptive filtering allows us to make the deformation in a single step instead of two for SAD, once again improving the plausibility of the obtained deformation field. Nevertheless, for extreme cases where we need to apply the modified algorithm of Section IV-D, we also need to relax the regularization and resort to a two-step approach.

The main hypotheses of our method are that the lesion expands radially and that there is no infiltration and no edema. Therefore, only meningiomas have been considered in this paper. Even though edema may be associated with meningiomas, no edema was present in the cases we present. Other—potentially more complex—models of growth and infiltration should obviously be considered for other types of tumors and lesions, but this is beyond the scope of this paper. On the other hand, let us consider the clinical relevance of our model for meningiomas: even if the vectors of growth of space-occupying lesions are not precisely known, it seems reasonable to assume from a biological point of view that homogeneous intra cerebral tumors (totally solid or totally cystic) have a radial growth. This is confirmed radiologically in cases where follow up of such lesions is performed. Regarding meningiomas, growth may be considered spatially homogeneous at least into directions where they are not restrained by anatomical structures like bone, cerebral falx or tentorium. Actually a large majority of meningiomas have a dural attachment and dura, except the falx and tentorium, is adherent to bone. As bone is rigid, it is reasonable to consider that there is no growth into the bone direction, even if bone may be invaded in rare cases. In conclusion, it is realistic to assume from a biological point of view that growth of meningiomas is radial and starts from the center of their dural attachment surface, defined as the seeding point.

The seed position has to be manually chosen by an expert. That represents a drawback because our results clearly show that the brain deformation induced by the lesion growth is correlated with the position of the seeding point (see discussion in Section V-B). Actually, this observation is not surprising considering that we assume a radial growth. Furthermore, the best deformation accuracy is not necessarily obtained when seeding point is *logically* placed in the center of the surface of dural attachment (see Fig. 14). As a proof, our two first

(a) Segmented structures: Ventricles   (b) Segmented structures: Thalamus
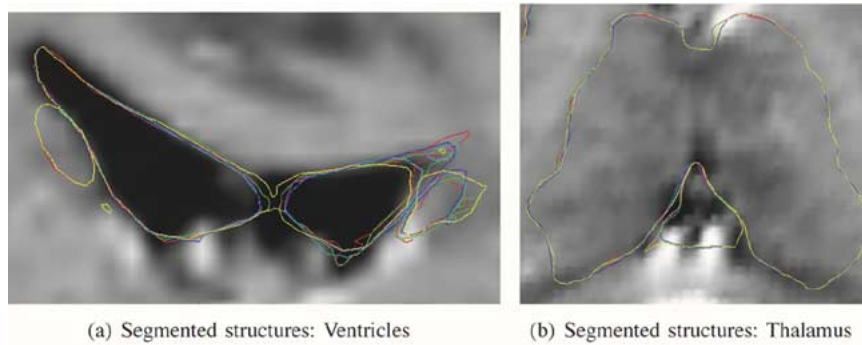
Fig. 16. Segmentation results for each seed position: zoom at ventricles and thalamus area. (a) Segmented structures: ventricles. (b) Segmented structures: thalamus.

TABLE I
VOLUME MEASURE OF SEGMENTED STRUCTURES FOR EACH SEED POSITION. VOLUME AND STATISTICS ARE IN mm^3. PERCENTAGE VALUES ARE CALCULATED RESPECT TO THE MEAN VALUE. MSE IS THE MEAN SQUARE ERROR PER VOXEL BETWEEN THE ORIGINAL PATIENT AND THE DEFORMED SYNTHETIC ATLAS-PATIENT INTENTITIES

| Seed position	Tumor	Ventricles	Central Nuclei	Thalamus	MSE
(192,119,38)	33168.60	19133.40	12851.52	10115.16	35.73
(205,131,50)	33302.28	19054.20	12801.36	10091.40	42.50
(205,136,47)	33040.92	19256.16	12726.12	10072.92	34.08
(205,137,57)	33365.64	19171.68	12728.76	10087.44	37.01
(206,139,53)	33249.48	19170.36	12732.72	10080.84	37.50
(207,145,48)	33333.96	19110.96	12773.64	10071.60	36.30
Mean	33291.72	19149.24	12769.20	10086.12	37.19
Standard deviation	62.92 (0.18%)	68.01 (0.35%)	50.30 (0.03%)	16.02 (0.15%)	2.86 (7.69%)
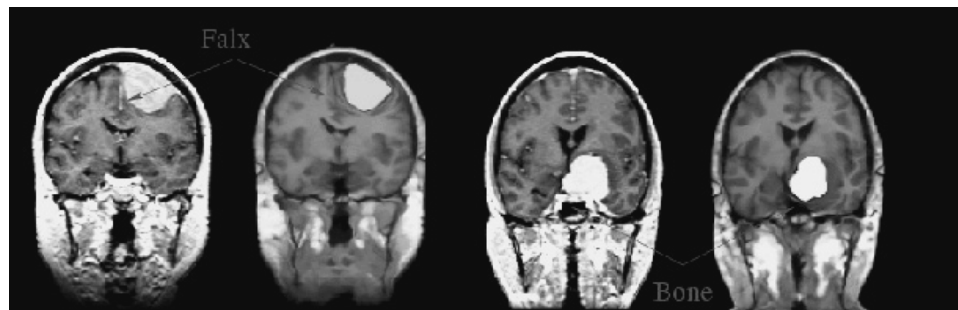
Fig. 17. Deformation errors for patient 1 and 2. Falx and bone have been too much deformed since there are no special constraints of deformation for such structures while they have in fact much less elasticity than the rest of the brain.

cases, patient 1 and patient 2, show no shift of neither the falx nor the *sella turcica* (bone) despite the presence of the meningioma while the corresponding deformed images by the MLG method have deformed these structures (see Fig. 17). Actually, falx and tentorium, although less rigid than bone, have significantly higher resistances against tumor growth than brain. So, we should also consider them like nondeformable structures almost until the tumor reaches a significant size. Consequently, in a future work, the algorithm will be modified in order to prevent too much deformability of these structures rendering the algorithm less dependent of finding the exact initial seed position. Injecting a contrast product is very useful in clinical practise to appreciate the anatomical limits of tumors since most of them, including meningiomas, are iso-intense on noncontrasted T1-weighted MR images. However, enhanced brain structures like vessels, choroid plexus, meninges, and vascularized tissues like sinus mucosae appear with different intensities in patients than in atlas images, where contrast is not injected. Thus, this effect should be also considered to avoid

possible problems (for instance, too much deformability of some structures) when applying the nonrigid registration since an optical flow method is used that assumes that the intensity does not change between images. In fact, in the areas where the contrast product is present, the strong gradient intensity in the reference image and also large intensity difference between the reference and the deformable images cause too large deformations. A possible solution would be to create the same contrast effect in the atlas proceeding first by segmenting the *meninges* and *sinuses* and simulating the same intensity as in the patient image. So there would be a perfect intensity correspondence and no errors in these regions will be performed.

Considering all the possible space-occupying lesions in a unified framework is almost impossible. Thus, different models could be related to specific pathologies taking into account both pushing and infiltrating effects as well as edema. On the other side, the proposed method could be applied to ischemic lesions like stroke (chronic phase) where surrounding brain tissue is attracted rather than pushed by the lesion.

Now, the method should be tested on more data sets containing different kind and size of lesions in order to better validate. Also, it would be important to study a case where the lesion evolution is known to see if the model of lesion growth we have proposed is near or far from the reality.

Finally, in a more evolved method it would be also very important to consider some anatomical constraints of the structures of interest introducing for example some shape analysis of the most important structures near the lesion as well as to take into account the existence of the edema.

VII. CONCLUSION

We proposed a new approach for brain atlas deformation in the presence of large space-occupying tumors, which makes use of a simple model of tumor growth. We first compared our method to the most similar methods found in the literature. Results show that limitations of other methods have been overcame thanks to the use of an *a priori* model and that a good matching is obtained in pathological brains, even when some structures have been drastically altered by the presence of a tumor. We proposed also a new validation method to analyze not only the lesion growth but also the most probable origin of the tumor. Finally, we deeply discussed the weak points of our method and proposed some solutions to overcome these limitations.

ACKNOWLEDGMENT

REFERENCES

[1] S. K. Kyriacou and C. Davatzikos, "Nonlinear elastic registration of brain images with tumor pathology using a biomechanical model," *IEEE Trans. Med. Imag.*, vol. 18, pp. 580–592, July 1999.

[2] B. M. Dawant, S. L. Hartmann, and S. Gadamsetty, "Brain atlas deformation in the presence of large space-occupying tumors," in *Proc. 2nd Int. Conf. Medical Image Computing and Computer-Assisted Intervention*, 1999, pp. 589–596.

[3] J.-P. Thirion, "Image matching as a diffusion process: An analogy with Maxwell's demons," *Med. Image Anal.*, vol. 2, no. 3, pp. 243–260, 1998.

[4] M. Bach Cuadra, J. Gomez, P. Hagmann, C. Pollo, J.-G. Villemure, B. M. Dawant, and J.-P. Thiran, "Atlas-based segmentation of pathological brains using a model of tumor growth," in *Proc. 2nd Int. Conf. Medical Image Computing and Computer-Assisted Intervention*, 2002, pp. 380–387.

[5] A. W. Toga, *Brain Warping*. Orlando, FL: Academic, 1999.

[6] J.-P. Thirion, "Fast non-rigid matching of 3D medical images," INRIA, Tech. Rep. 2547, May 1995.

[7] P. Cachier, X. Pennec, and N. Ayache, "Fast non-rigid matching by gradient descent: Study and improvements of the "demons" algorithm," INRIA, Tech. Rep. 3706, June 1999.

[8] M. Bach Cuadra, "Atlas-based segmentation and classification of magnetic resonance brain images," Ph.D. dissertation, Swiss Federal Inst. Technol., Lausanne, Switzerland, Nov. 2003.

[9] O. Cuisenaire, J.-P. Thiran, B. Macq, C. Michel, A. D. Volder, and F. Marques, "Automatic registration of 3D MR images with a computerized brain atlas," *SPIE Med. Imag.*, vol. 1719, pp. 438–449, 1996.

[10] P. Schroeter, "Unsupervised two-dimensional and three-dimensional image segmentation," Ph.D. dissertation, Swiss Federal Inst. Technol., Lausanne, Switzerland, 1996.

[11] S. K. Warfield, M. Kaus, F. A. Jolesz, and R. Kikinis, "Adaptive, template moderated, spatially varying statistical classification," *Med. Image Anal.*, vol. 4, pp. 43–55, Mar. 2000.

[12] M. R. Kaus, S. K. Warfield, A. Nabavi, E. Chatzidakis, P. M. Black, F. A. Jolesz, and R. Kikinis, "Segmentation of meningiomas and low grade gliomas in MRI," in *Proc. 2nd Int. Conf. Medical Image Computing and Computer-Assisted Intervention*, 1999, pp. 1–10.

[13] J. Gomez, "Brain atlas registration in presence of brain lesions," M.S. thesis, Swiss Federal Inst. Technol., Lausanne, Switzerland, [Online]. Available: http://ltswww.epfl.ch/~bach/RefsTMI/Jesus-GomezDiploma.pdf, 2001.

[14] S. K. Warfield *et al.*. NSG brain tumor database. [Online]. Available: http://spl.bwh. harvard.edu:8000/~warfield/tumorbase/

[15] R. Kikinis *et al.*, "A digital brain atlas for surgical planning, model driven segmentation and teaching," *IEEE Trans. Vis. Comput. Graph.*, vol. 2, pp. 232–241, Sept. 1996.

[16] S. K. Warfield *et al.*, "A binary entropy measure to assess nonrigid registration algorithms," in *Proc. 2nd Int. Conf. Medical Image Computing and Computer-Assisted Intervention*, 2001, pp. 266–274.

[17] P. Hellier *et al.*, "Retrospective evaluation of inter-subject brain registration," in *Proc. 2nd Int. Conf. Medical Image Computing and Computer-Assisted Intervention*, 2001, pp. 258–265.

[18] J. West *et al.*, "Comparison and evaluation of retrospective intermodality brain image registration techniques," *J. Comput. Assist. Tomogr.*, 1996.

[19] *Numerical Recipes in C, The Art of Scientific Computing*. Cambridge, U.K.: Cambridge Univ. Press.